# Upconversion and Downconversion Fluorescent Graphene Quantum Dots: Ultrasonic Preparation and Photocatalysis

**Shujuan Zhuo,[†,‡] Mingwang Shao,[†,*] and Shuit-Tong Lee[§,*]**

[†]Institute of Functional Nano & Soft Materials (FUNSOM) and Jiangsu Key Laboratory for Carbon-Based Functional Materials & Devices, Soochow University, Suzhou, Jiangsu 215123, People's Republic of China, [‡]Anhui Key Laboratory of Functional Molecular Solids, College of Chemistry and Materials Science, Anhui Normal University, Wuhu 241000, People's Republic of China, and [§]Center of Super-Diamond and Advanced Films and Department of Physics and Materials Science, City University of Hong Kong, Hong Kong SAR, People's Republic of China

**ABSTRACT** A facile ultrasonic route for the fabrication of graphene quantum dots (GQDs) with upconverted emission is presented. The as-prepared GQDs exhibit an excitation-independent downconversion and upconversion photoluminescent (PL) behavior, and the complex photocatalysts (rutile $TiO_2$/GQD and anatase $TiO_2$/GQD systems) were designed to harness the visible spectrum of sunlight. It is interesting that the photocatalytic rate of the rutile $TiO_2$/GQD complex system is *ca.* 9 times larger than that of the anatase $TiO_2$/GQD complex under visible light ($\lambda > 420$ nm) irradiation in the degradation of methylene blue.

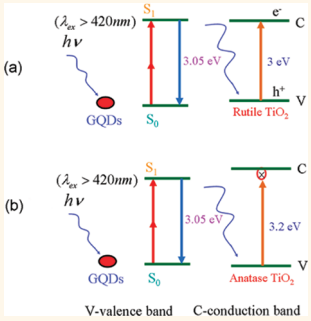


**KEYWORDS:** graphene quantum dots · upconversion luminescence · photocatalysts

Recently, graphene has received much attention because of its many unique and novel properties,[1−4] such as superior mechanical flexibility, excellent thermal/chemical stability, and environmentally friendly nature. Compared to two-dimensional graphene nanosheets and one-dimensional nanoribbons, zero-dimensional graphene quantum dots (GQDs) possess strong quantum confinement and edge effects when their sizes are down to 10 nm, which induce new physical properties.[5−9] Hence, GQDs have potential application in many fields, such as photovoltaics, bioimaging, light-emitting diodes, and sensors.[10,11]

However, the development and application of GQDs remain inchoate, and the synthesis is only a recent effort. Very recently, Pan and co-workers[12] have developed a hydrothermal route for cutting preoxidized graphene sheets into GQDs (9.6 nm in average diameter) with blue emissions. Li and colleagues[13] presented an electrochemical approach for direct preparation of functional GQDs with a uniform size of 3−5 nm as potential electron acceptors for photovoltaics. Shen *et al.* proposed a hydrazine hydrate reduction of graphene oxide method for the fabrication of GQDs with upconverted emission.[14] However, the produced GQDs with above-mentioned methods exhibit an excitation-dependent PL behavior.

Herein, we presented a new facile ultrasonic method to prepare GQDs, which exhibited bright PL in a water solution. Most interestingly, the as-prepared GQDs possessed excitation-independent downconversion and upconversion PL properties. The PL spectra showed a strong peak at 407 nm. Significantly, we demonstrated the design of photocatalysts (rutile $TiO_2$/GQD and anatase $TiO_2$/GQD complex systems) to harness the visible spectrum of sunlight, based on the upconversion luminescence properties of GQDs. The essential difference of these systems is that rutile $TiO_2$ possesses narrower band gap than 407 nm and anatase $TiO_2$ wider than 407 nm. Their photocatalytic ability was determined by degradation of methylene blue (MB) under Xe lamp irradiation (with 420 nm cutoff filter), owing to its well-established mechanistic pathway of degradation (Figure S1 in Supporting Information).[15] The results showed that the photocatalytic rate of the rutile $TiO_2$/GQD complex system is *ca.* 9 times larger than that of the anatase $TiO_2$/GQD one. Furthermore, the preliminary mechanism of excitation-independent downconversion and upconversion PL behavior

* Address correspondence to mwshao@suda.edu.cn, apannale@cityu.edu.hk.

Received for review July 22, 2011 and accepted January 5, 2012.

**Published online January 05, 2012**
**10.1021/nn2040395**

and excellent photocatalytic activities based on rutile $TiO_2$/GQD complex was proposed.

## RESULTS AND DISCUSSION

Figure 1 shows the TEM images of as-prepared monodisperse GQDs with diameters of 3−5 nm (similar to that reported by Li *et al.*[13]). The SAED pattern of GQDs (Figure 1a, inset) reveals the clear diffraction ring of the GQD (100) crystal plane. Particularly, the present GQDs can freely disperse in water with transparent appearance without further ultrasonic dispersion.

The UV−vis absorption spectrum of GQDs in water shows an absorption band at *ca.* 300 nm (Figure 2). In the inset to Figure 2, a photograph of the dispersed GQDs illuminated under UV light (365 nm) is shown. The bright blue PL of GQDs is strong enough to be easily seen with the naked eye.

Raman spectroscopy of the GQDs is shown in Figure S2 (Supporting Information), which confirms the quality of the as-prepared GQDs. The G band at 1589 $cm^{-1}$ and D band at 1331 $cm^{-1}$ were observed, similar to that of blue luminescent hydrothermally synthesized GQDs.[12]

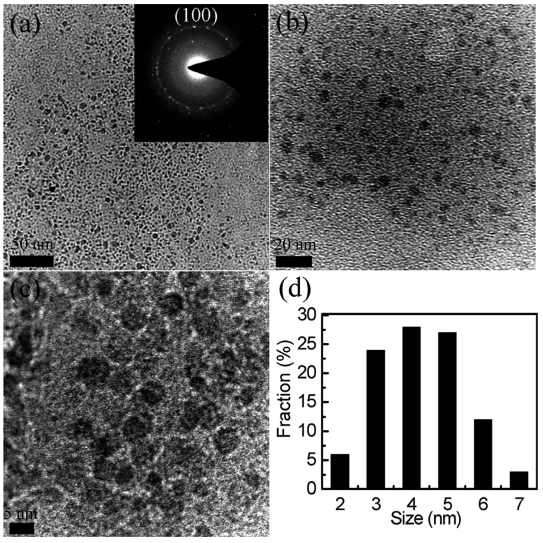


**Figure 1. (a−c) TEM images of as-prepared GQDs with different magnification; and (d) size distribution of GQDs. The inset in (a) is the SAED pattern of GQDs.**

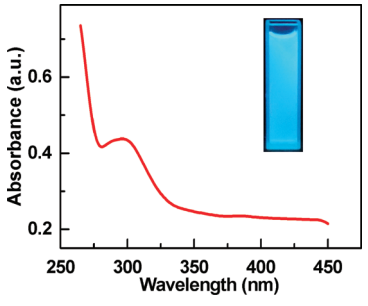


**Figure 2. UV−vis absorption spectrum of the GQDs dispersed in water. Inset: optical photograph of the GQDs dispersed in water illuminated under UV light (365 nm).**

To further explore the optical properties of as-synthesized GQDs, a detailed PL study was carried out by using different excitation wavelengths. Generally speaking, the PL spectra of most luminescent carbon nanoparticles are dependent on excitation wavelength. In other words, the PL peaks shifted to longer wavelengths with a maximum intensity as the excitation wavelength was a bathochromic shift. However, the as-prepared GQDs in this work show an excitation-independent PL feature. When the excitation wavelength changes from 240 to 340 nm, the PL spectra are almost invariable and show a strong peak at *ca.* 407 nm (Figure 3). Figure S3 (Supporting Information) shows the photoluminescence excitation spectrum of as-synthesized GQDs.

The above results indicate the GQDs indeed exhibit an excitation-independent PL behavior. Through literature research, it was found that the Yang group have presented a calculation method using a first-principle many-electron Green's function approach within the GW approximation to calculate the quasiparticle energies and band gaps of graphene nanoribbons (GNRs).[16] The results indicated that the calculated quasiparticle band gaps show significant self-energy corrections for both armchair and zigzag GNRs, in the range of 0.5−3.0 eV for ribbons of 2.4−0.4 nm width. According to the above theory, we calculate that the PL spectrum at 407 nm (3.05 eV) is corresponding to the ribbons of *ca.* 0.4 nm width (band gap 3.0 eV). Such tiny nanoribbons might come from the protrudent edge of GQDs synthesized by the ultrasonic route.

It is well-known that ultrasound can generate alternating low-pressure and high-pressure waves in liquid, leading to the formation and violent collapse of small vacuum bubbles. These cavitations cause high-speed impinging liquid jets, deagglomeration, and strong hydrodynamic shear forces.[17] Thus the energy of ultrasonic wave cuts graphene sheets into GQDs. During the cutting process, ultrasmall particles with a protrudent edge were formed.

In addition to the strong downconversion PL properties, remarkably, GQDs show a clear upconversion PL feature. Figure 4 shows the PL spectra of GQDs excited by long-wavelength light with the upconverted emissions located at *ca.* 407 nm, which is the same as the

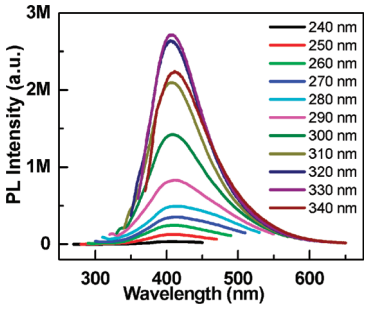


**Figure 3. PL spectra of the GQDs at different excitation wavelengths.**

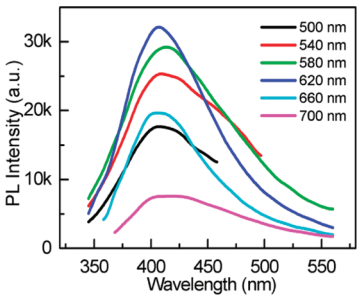


**Figure 4. Upconverted PL spectra of the GQDs at different excitation wavelengths.**

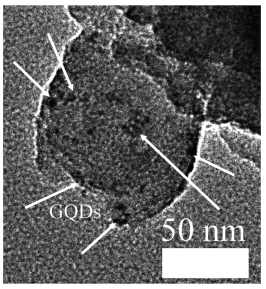


**Figure 5. TEM image of rutile $TiO_2$/GQD nanocomposites: the GQDs are marked with white arrows.**

downconversion PL peak. Most interestingly, similar to the downconversion PL spectra, the upconversion PL also show an excitation-independent PL behavior. The PL spectra are almost unchanged and show a strong peak at *ca.*407 nm with the excitation wavelength red shift (from 500 to 700 nm). The upconverted PL property of GQDs should be attributed to the multiphoton active process similar to previous reported carbon dots.[18,19]

To determine the upconversion luminescence efficiency of GQDs, the absolute quantum yield (QY) was measured using a fluorimeter and an integrating sphere (excitation wavelength, 620 nm). The QY of GQDs is determined to be 3.4%.

The above results indicated that GQDs might be employed for full use of the visible spectrum of sunlight, combined with wide band gap photocatalysts.

$TiO_2$ is the most widely used photocatalyst,[20,21] but its limited activity under visible light irradiation due to wide intrinsic band gap has motivated the quest for modified $TiO_2$ materials to absorb visible light. Considering the upconversion properties of GQDs, we expected that combining GQDs with $TiO_2$ in a composite system for photocatalysis would realize the efficient usage of the visible spectrum of sunlight.

Figure 5 shows the TEM image of rutile $TiO_2$/GQD nanocomposites, indicating that GQDs (marked with white arrows) are attached to the surfaces of the $TiO_2$. To further confirm the formation of the composite structure, the SEM image and EDS element mapping of rutile $TiO_2$/GQD nanocomposites were obtained and are shown in Figure 6. EDS element mapping clearly

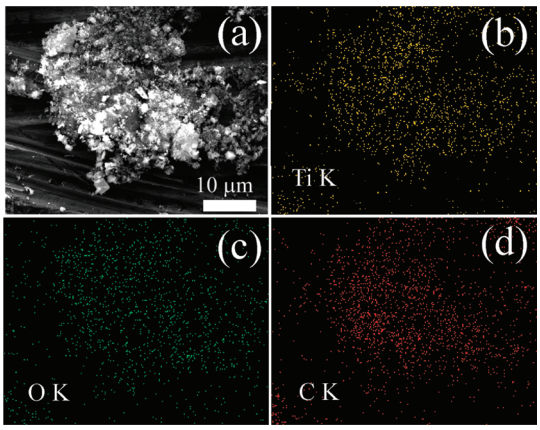


**Figure 6. (a) SEM image of rutile $TiO_2$/GQD composites; and EDS element mapping data of (b) Ti, (c) O, and (d) C elements throughout the $TiO_2$/GQD composites.**

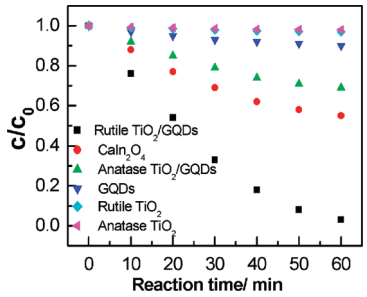


**Figure 7. Relationship between MB concentration and reaction time for different catalysts: rutile $TiO_2$/GQDs, $CaIn_2O_4$, anatase $TiO_2$/GQDs, GQDs, rutile $TiO_2$ NPs, and anatase $TiO_2$ NPs.**

shows the elements of Ti, O, and C evenly distributed in the $TiO_2$/GQD composites.

The photocatalytic ability was determined by degradation of MB under visible light irradiation. Figure 7 shows the concentration of the aqueous MB solution *versus* irradiation time. As can be seen, the photodegradation efficiency is up to 97% in 60 min with the rutile $TiO_2$/GQD complex acting as photocatalyst. However, the efficiency is only 31% with anatase $TiO_2$/GQD catalysts.

The anatase phase usually has much higher photocatalytic ability than rutile $TiO_2$ does.[22] It is more interesting that the activity of the rutile $TiO_2$/GQD complex is evidently superior to that of the anatase $TiO_2$/GQD one. The possible reason might be explained as follows: in photocatalysis, a semiconductor absorbs energy equal to or larger than its band gap to form electron/hole ($e^-/h^+$) pairs. Under visible light ($\lambda >$ 420 nm) irradiation, the upconverted PL peak of GQDs is located at *ca.* 407 nm (3.05 eV). This energy is larger than the band gap of rutile $TiO_2$ 3.0 eV (414 nm), yet smaller than that of anatase $TiO_2$ 3.2 eV (388 nm). That is, the upconversion PL emission of GQDs only excited rutile $TiO_2$ to form $e^-/h^+$ pairs. Hence the photocatalytic ability of rutile $TiO_2$/GQD is much superior to that

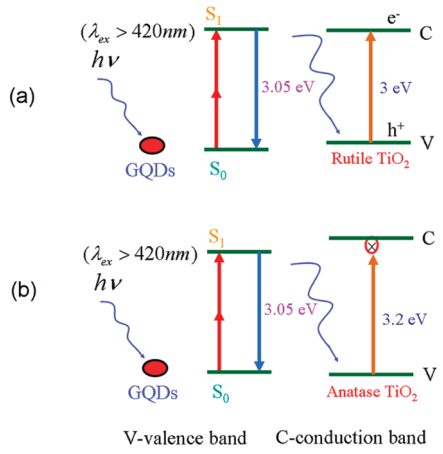


**Figure 8. Schematic of photocatalytic process for (a) rutile $TiO_2$/GQD and (b) anatase $TiO_2$/GQD under visible light ($\lambda$ > 420 nm) irradiation.**

of the anatase $TiO_2$/GQD complex. The aforementioned process is schematically shown in Figure 8.

For comparison, contrast experiments were carried out using only pure rutile $TiO_2$ (50 mg), pure anatase $TiO_2$ (50 mg), or pure GQDs (5 mL) as photocatalysts, and little reduction of MB was observed, which indicated that the excellent photocatalytic activities of $TiO_2$/GQD should be attributed to the interaction between GQDs and $TiO_2$.

The photocatalytic activity of $CaIn_2O_4$ was also examined for comparison. $CaIn_2O_4$ is a visible light photocatalyst absorbing wavelengths shorter than 480 nm with an indirect band gap for optical transitions.[23] The $CaIn_2O_4$ catalysts in this experiment were prepared by solid-state reaction with the method reported before.[24] The XRD pattern of the as-prepared $CaIn_2O_4$ is shown in Figure S4 (Supporting Information), and all diffraction peaks may be indexed as the orthorhombic phase of $CaIn_2O_4$ (JCPDS card no. 17-0643), which confirms the quality of the products. As shown in Figure 7, the photodegradation efficiency is up to 45% in 60 min with $CaIn_2O_4$ (50 mg) as photocatalyst, which is larger than that of anatase $TiO_2$/GQDs, yet smaller than that of rutile $TiO_2$/GQDs.

Most of the photocatalytic reactions follow the Langmuir–Hinshelwood adsorption model,[25] and the L–H model can be simplified to a pseudo-first-order expression: $\ln(C_0/C) = kt$ (where $C_0$ and $C$ are the equilibrium concentration of adsorption and the concentration of MB at the exposure time, $t$, respectively, and $k$ is the apparent rate constant). Using regression-fitting techniques, the linear plots of $\ln(C_0/C)$ *versus* irradiation time $t$ are attained. Table 1 summarizes the calculated $k$ and the corresponding correlation coefficient ($R$) values. As can be seen from Table 1, the apparent rate constants are 0.0576, 0.0063, 0.0017, 0.0005, 0.0003, and 0.01016 $min^{-1}$ for rutile $TiO_2$/GQD, anatase $TiO_2$/GQD, GQDs, rutile $TiO_2$, anatase $TiO_2$, and $CaIn_2O_4$, respectively. Hence, the photocatalytic reaction rate of rutile

**TABLE 1. Degradation Rate Constants of MB with Different Catalysts Using $\ln(C_0/C) = kt$ as Fitting Equation**

| photocatalysts | linear equation | $k$ ($min^{-1}$) | $R$ |
|---|---|---|---|
| rutile $TiO_2$/GQD | $\ln(C_0/C) = 0.0576t - 0.3349$ | 0.0576 | 0.977 |
| anatase $TiO_2$/GQD | $\ln(C_0/C) = 0.0063t + 0.02411$ | 0.0063 | 0.987 |
| GQDs | $\ln(C_0/C) = 0.0017t + 0.0115$ | 0.0017 | 0.979 |
| rutile $TiO_2$ | $\ln(C_0/C) = 0.0005t + 0.0038$ | 0.0005 | 0.972 |
| anatase $TiO_2$ | $\ln(C_0/C) = 0.0003t + 0.00292$ | 0.0003 | 0.967 |
| $CaIn_2O_4$ | $\ln(C_0/C) = 0.01016t + 0.03541$ | 0.01016 | 0.989 |

$TiO_2$/GQD is *ca.* 9 times larger than that of anatase $TiO_2$/GQD and 5.7 times larger than that of $CaIn_2O_4$.

To further demonstrate the effect of GQDs on the photocatalytic activity of composites, photocatalytic degradation of MB using the Xe light source without the 420 nm cutoff filter was carried out and shown in Figure S5 (Supporting Information), and the photodegradation efficiencies for different catalysts were all improved to some extent. The efficiency can be up to 99% with the rutile $TiO_2$/GQD complex and 58% with the anatase $TiO_2$/GQD one. The apparent rate constants are 0.07289, 0.0143, 0.00395, 0.00347, and 0.0032 $min^{-1}$ for rutile $TiO_2$/GQDs, anatase $TiO_2$/GQDs, GQDs, rutile $TiO_2$, and anatase $TiO_2$, respectively (Table S1, Supporting Information). The photocatalytic reaction rate of rutile $TiO_2$/GQDs is *ca.* 5 times larger than that of anatase $TiO_2$/GQDs, which confirms the important role of upconversion luminescence GQDs on the process of photocatalytic reactivity.

Photocurrents were measured for rutile $TiO_2$/GQD, anatase $TiO_2$/GQD, rutile $TiO_2$, and anatase $TiO_2$ to investigate the electronic interaction between $TiO_2$ and GQDs (Figure S6, Supporting Information). It was clear that fast and uniform photocurrent responses were observed in all materials, and the photoresponsive phenomenon was entirely reversible. Under visible light irradiation ($\lambda$ > 420 nm), the photocurrent of the rutile $TiO_2$/GQD material was *ca.* 2.6 times higher than that of the anatase $TiO_2$/GQD material. The photocurrent enhancement of the rutile $TiO_2$/GQD photocatalyst indicated an enhanced photoinduced electron and hole separation, which might induce the improvement of photocatalytic activity.[26] Pure rutile $TiO_2$ and anatase $TiO_2$ showed almost no photocurrent response.

Surface photovoltage (SPV) measurements were conducted to further investigate the photocatalytic ability of the $TiO_2$/GQD nanocomposite. SPV is the difference in surface potential before and after illumination for semiconductor materials, which could be used to study the separation and transfer behavior of photogenerated charge carriers. Unlike the UV–vis spectra, which cover all types of photon absorption, the SPV spectra are only sensitive to the electron transition-related process and subsequent charge separation. The higher SPV signal may suggest the higher separation rate of

photogenerated charge carriers.[27] The rutile $TiO_2$/GQD photocatalyst exhibits distinguished SPV response (Table S2, Supporting Information), and its performance is evidently higher than those of the other photocatalysts, which means that the charge separation efficiency is the highest for rutile $TiO_2$/GQDs. Therefore, the photocatalytic activity is the best for rutile $TiO_2$/GQDs.

## CONCLUSIONS

In summary, GQDs with excellent PL properties were conveniently synthesized using a direct and simple ultrasonic reaction process. The as-prepared GQDs exhibited an extraordinary excitation-independent PL behavior. The complex photocatalysts (rutile $TiO_2$/GQD and anatase $TiO_2$/GQD systems) were designed to harness the visible spectrum of sunlight, based on the upconversion PL properties of GQDs. The results indicated that the photocatalytic activities of the rutile $TiO_2$/GQD complex are obviously superior to that of the anatase $TiO_2$/GQD one. For conserving energy and being environmentally benign, these GQDs would offer great potential for a broad range of applications, including biosensors, bioimaging, laser, and light-emitting diodes. They also might serve as a promising candidate for a new type fluorescence marker, as well as a new approach to high-efficiency catalyst design for applications in bioscience and energy technology.

## METHODS

**Materials.** Graphene was purchased from Ningbo Institute of Materials Technology & Engineering Chinese Academy of Sciences (China). Rutile and anatase titania nanoparticles (50 nm in average diameter) were purchased from Shanghai Jiang Hu Titania Company (China). Other reagents were of analytical reagent grade and were used without further purification. Doubly distilled water was used throughout the work.

**Preparation of GQDs.** Graphene (0.05 g) was oxidized in concentrated $H_2SO_4$ (10 mL) and $HNO_3$ (30 mL) at room temperature for 12 h. Then the mixed solution was subsequently treated ultrasonically for 12 h with an ultrasonic instrument (model KQ-300 TDE, 300 W, 80 kHz). The mixture was calcined in a furnace installed with an exhaust gas recovery at 350 °C for 20 min to remove the concentrated $H_2SO_4$ (boiling point, 338 °C) and $HNO_3$ (boiling point, 83 °C). The as-prepared products were redispersed in water (40 mL). Then the resulting black suspension was filtered through a 0.22 $\mu$m microporous membrane to get a brown filter solution. This solution was further dialyzed in a dialysis bag (retained molecular weight: 3500 Da) overnight to obtain GQDs.

**Characterization.** The transmission electron microscopy (TEM) and selected area electron diffraction (SAED) patterns were taken with a Tecnai $G^2$ F20 transmission electron microscope operating at 200 kV. Scanning electron microscopy (SEM) image and energy-dispersive X-ray (EDS) element mapping were taken on a FEI-quanta 200 scanning electron microscope. Fluorescence spectra were measured with a Fluoromax-4 spectrofluorimeter. Raman spectrum was collected on an HR 800 Raman spectroscope (JY, France) equipped with a synapse CCD detector and a confocal Olympus microscope. The spectrograph uses 600 g/mm gratings and a 633 nm He−Ne laser. The UV−vis absorption spectrum was recorded on a Perkin-Elmer Lambda 750 spectrophotometer. X-ray powder diffraction (XRD) was carried out on a Philips X'pert PRO MPD diffractometer with Cu K$\alpha$ radiation ($\lambda$ = 0.15406 nm). The upconversion luminescence efficiency was measured with a Horiba Jobin Yvon FL-1057 spectrofluorimeter with a barium sulfate coated integrating sphere. Photovoltage and photocurrent experiments were conducted on a Newport 91160 solar simulator equipped with a 300 W xenon lamp, and an air mass (AM) 1.5 filter was used to generate simulated AM 1.5 solar spectrum irradiation source with a 420 nm cutoff filter to provide visible light. Fluorine-doped $SnO_2$ (FTO) conducting glass was chosen as the electrode substrates. The signal from the sample was detected using a sandwich-like structure of FTO/sample/FTO. The electrolyte is composed of mixed ionic liquid, the 1-ethyl-3-methylimidazolium thiocyanate (EMISCN) and 1-propyl-3-methylimidazolium iodide (PMII) (EMISCN/PMII = 7:13, v/v). The illumination area of the electrode was about 0.12 $cm^2$. All of the electrical data were recorded with a Keithley 2612 source meter.

**Photocatalytic Degradation of MB.** Rutile or anatase $TiO_2$ nanoparticles (50 mg) were added to GQD solution (5 mL) with stirring for 30 min and dried in a vacuum oven at 65 °C for 8 h to give the $TiO_2$/GQD nanocomposite. The photocatalytic degradation reaction was carried out at room temperature under ambient conditions by adding different photocatalysts to 50 mL of aqueous MB solution with an initial concentration of $2 \times 10^{-5}$ M. Prior to illumination, the suspension was protected from light and magnetically stirred for 6 h to reach adsorption equilibrium. A 350 W Xe lamp was used as a light source with a 420 nm cutoff filter to provide visible light irradiation. The distance between the light and solution was about 5 cm. At given intervals, 1 mL of the suspension was extracted and centrifuged for 15 min. The UV−vis absorption spectra of the supernatant were then measured. MB was determined spectrophotometrically at $\lambda_{max}$ = 664 nm. The photocatalytic degradation efficiency of MB was calculated by the formula $E = (A_0 - A)/A_0 \times 100\%$, where $A_0$ was the adsorption equilibrium absorbance of MB and $A$ was the absorbance of MB solution at irradiation time, $t$.

*Acknowledgment.* This work was supported by the National Natural Science Foundation of China (NSFC) (Nos. 21071106, 91027041) and Specialized Research Fund for the Doctoral Program of Higher Education (20103201110016).

*Supporting Information Available:* Photocatalytic degradation pathway of MB, Raman spectroscopy of the GQDs, PLE spectrum of the GQDs, XRD pattern of $CaIn_2O_4$, relationship between MB concentration and reaction time for different catalysts under Xe light source without the 420 nm cutoff filter, the degradation rate constants of MB with different catalysts under Xe light source without the 420 nm cutoff filter, photocurrent response curves and photovoltage data of rutile $TiO_2$/GQD, anatase $TiO_2$/GQD, rutile $TiO_2$, and anatase $TiO_2$ materials under visible light irradiation ($\lambda$ > 420 nm). This material is available free of charge *via* the Internet at http://pubs.acs.org.

## REFERENCES AND NOTES

1. Rafiee, M. A.; Lu, Wei.; Thomas, A. V.; Zandiatashbar, A.; Javad, R.; Tour, J. M.; Koratkar, N. A. Graphene Nanoribbon Composites. *ACS Nano* **2010**, *4*, 7415–7420.
2. Myung, S.; Solanki, A.; Kim, C.; Park, J.; Kim, K. S.; Lee, K. B. Graphene-Encapsulated Nanoparticle-Based Biosensor for the Selective Detection of Cancer Biomarkers. *Adv. Mater.* **2011**, *23*, 2221–2225.
3. Hu, W. B.; Peng, C.; Luo, W. J.; Lv, M.; Li, X. M.; Li, D.; Huang, Q.; Fan, C. H. Graphene-Based Antibacterial Paper. *ACS Nano* **2010**, *4*, 4317–4323.

4. Geim, A. K. Graphene: Status and Prospects. *Science* **2009**, *324*, 1530–1534.
5. Yan, X.; Cui, X.; Li, B. S.; Li, L. S. Large, Solution-Processable Graphene Quantum Dots as Light Absorbers for Photovoltaics. *Nano Lett.* **2010**, *10*, 1869–1873.
6. Ponomarenko, L. A.; Schedin, F.; Katsnelson, M. I.; Yang, R.; Hill, E. W.; Novoselov, K. S.; Geim, A. K. Chaotic Dirac Billiard in Graphene Quantum Dots. *Science* **2008**, *320*, 356–358.
7. Girit, C. O.; Meyer, J. C.; Erni, R.; Rossell, M. D.; Kisielowski, C.; Yang, L.; Park, C. H.; Crommie, M. F.; Cohen, M. L.; Louie, S. G.; *et al.* Graphene at the Edge: Stability and Dynamics. *Science* **2009**, *323*, 1705–1708.
8. Yan, X.; Cui, X.; Li, L. S. Synthesis of Large, Stable Colloidal Graphene Quantum Dots with Tunable Size. *J. Am. Chem. Soc.* **2010**, *132*, 5944–5945.
9. Guo, C. X.; Yang, H. B.; Sheng, Z. M.; Lu, Z. S.; Song, Q. L.; Li, C. M. Layered Graphene/Quantum Dots for Photovoltaic Devices. *Angew. Chem., Int. Ed.* **2010**, *49*, 3014–3017.
10. Geng, X. M.; Niu, L.; Xing, Z. Y.; Song, R. S.; Liu, G. T.; Sun, M. T.; Cheng, G. S.; Zhong, H. J.; Liu, Z. H.; Zhang, Z. J.; *et al.* Aqueous-Processable Noncovalent Chemically Converted Graphene−Quantum Dot Composites for Flexible and Transparent Optoelectronic Films. *Adv. Mater.* **2010**, *22*, 638–642.
11. Zhu, S. J.; Zhang, J. H.; Qiao, C. Y.; Tang, S. J.; Li, Y. F.; Yuan, W. J.; Li, B.; Tian, L.; Liu, F.; Hu, R.; *et al.* Strongly Green-Photoluminescent Graphene Quantum Dots for Bioimaging Applications. *Chem. Commun.* **2011**, *47*, 6858–6860.
12. Pan, D. Y.; Zhang, J. C.; Li, Z.; Wu, M. H. Hydrothermal Route for Cutting Graphene Sheets into Blue-Luminescent Graphene Quantum Dots. *Adv. Mater.* **2010**, *22*, 734–738.
13. Li, Y.; Hu, Y.; Zhao, Y.; Shi, G. Q.; Deng, L. E.; Hou, Y. B.; Qu, L. T. An Electrochemical Avenue to Green-Luminescent Graphene Quantum Dots as Potential Electron-Acceptors for Photovoltaics. *Adv. Mater.* **2011**, *23*, 776–780.
14. Shen, J. H.; Zhu, Y. H.; Chen, C.; Yang, X. L.; Li, C. Z. Facile Preparation and Upconversion Luminescence of Graphene Quantum Dots. *Chem. Commun.* **2011**, *47*, 2580–2582.
15. Houas, A.; Lachheb, H.; Ksibi, M.; Elaloui, E.; Guillard, C.; Herrmann, J. M. Photocatalytic Degradation Pathway of Methylene Blue in Water. *Appl. Catal., B* **2001**, *31*, 145–157.
16. Yang, L.; Park, C. H.; Son, Y. W.; Cohen, M. L.; Louie1, S. G. Quasiparticle Energies and Band Gaps in Graphene Nanoribbons. *Phys. Rev. Lett.* **2007**, *99*, 186801.
17. Li, H. T.; He, X. D.; Liu, Y.; Huang, H.; Lian, S. Y.; Lee., S. T.; Kang, Z. H. One-Step Ultrasonic Synthesis of Water-Soluble Carbon Nanoparticles with Excellent Photoluminescent Properties. *Carbon* **2011**, *49*, 605–609.
18. Cao, L.; Wang, X.; Meziani, M. J.; Lu, F.; Wang, H.; Luo, P. G.; Lin, Y.; Harruff, B. A.; Veca, L. M.; Murray, D.; *et al.* Carbon Dots for Multiphoton Bioimaging. *J. Am. Chem. Soc.* **2007**, *129*, 11318–11319.
19. Li, H. T.; He, X. D.; Kang, Z. H.; Huang, H.; Liu, Y.; Liu, J. L.; Lian, S. Y.; Tsang, C. H. A.; Yang, X. B.; Lee, S. T. Water-Soluble Fluorescent Carbon Quantum Dots and Photocatalyst Design. *Angew. Chem., Int. Ed.* **2010**, *49*, 4430–4434.
20. Primo, A.; Corma, A.; García, H. Titania Supported Gold Nanoparticles as Photocatalyst. *Phys. Chem. Chem. Phys.* **2011**, *13*, 886–910.
21. Zhang, X. Y.; Li, H. P.; Cui, X. L.; Lin, Y. Graphene/$TiO_2$ Nanocomposites: Synthesis, Characterization and Application in Hydrogen Evolution from Water Photocatalytic Splitting. *J. Mater. Chem.* **2010**, *20*, 2801–2806.
22. Ismail, A. A.; Bahnemann, D. W. One-Step Synthesis of Mesoporous Platinum/Titania Nanocomposites as Photocatalyst with Enhanced Photocatalytic Activity for Methanol Oxidation. *Green Chem.* **2011**, *13*, 428–435.
23. Tang, J.; Zou, Z.; Katagiri, M.; Kako, T.; Ye, J. Photocatalytic Degradation of MB on $MIn_2O_4$ (M = Alkali Earth Metal) under Visible Light: Effects of Crystal and Electronic Structure on the Photocatalytic Activity. *Catal. Today* **2004**, *93−95*, 885–889.
24. Tang, J.; Zou, Z.; Ye, J. Effects of Substituting $Sr^{2+}$ and $Ba^{2+}$ for $Ca^{2+}$ on the Structural Properties and Photocatalytic Behaviors of $CaIn_2O_4$. *Chem. Mater.* **2004**, *16*, 1644–1649.
25. Bouzaza, A.; Laplanche, A. Photocatalytic Degradation of Toluene in the Gas Phase: Comparative Study of Some $TiO_2$ Supports. *J. Photochem. Photobiol. A* **2002**, *150*, 207–212.
26. Wang, Y. J.; Shi, R.; Lin, J.; Zhu, Y. F. Enhancement of Photocurrent and Photocatalytic Activity of ZnO Hybridized with Graphite-like $C_3N_4$. *Energy Environ. Sci.* **2011**, *4*, 2922–2929.
27. Liu, Z. Y.; Sun, D. D.; Guo, P.; Leckie, J. O. An Efficient Bicomponent $TiO_2/SnO_2$ Nanofiber Photocatalyst Fabricated by Electrospinning with a Side-By-Side Dual Spinneret Method. *Nano Lett.* **2007**, *7*, 1081–1085.